Global and Planetary Change 195 (2020) 103343

Contents lists available at ScienceDirect

Global and Planetary Change

journal homepage: www.elsevier.com/locate/gloplacha

Minimum carbon uptake controls the interannual variability of ecosystem productivity in tropical evergreen forests

Zhao Li[a,b], Anders Ahlström[b,c], Feng Tian[b,d], Antje Gärtner[b], Ming Jiang[a], Jianyang Xia[a,*]

[a] Zhejiang Tiantong Forest Ecosystem National Observation and Research Station, Research Center for Global Change and Ecological Forecasting, School of Ecological and Environmental Sciences, East China Normal University, Shanghai 200241, China
[b] Department of Physical Geography and Ecosystem Science, Lund University, Lund 223 62, Sweden
[c] Department of Earth System Science, School of Earth, Energy and Environmental Sciences, Stanford University, 473 Via Ortega, Stanford, CA 94305, USA
[d] School of Remote Sensing and Information Engineering, Wuhan University, Wuhan 430079, China

ARTICLE INFO

Keywords:
Carbon uptake
GPP
Inter-annual variability
Photosynthesis
Tropical evergreen forests
Minimum vegetation growth

ABSTRACT

Tropical evergreen forests contribute an important part to the interannual variability (IAV) of the global terrestrial gross primary productivity (GPP). Due to its year-round growing-season, high minimum carbon uptake (GPP_{min}) and dry season greening-up, the key processes driving the GPP variability across seasonal to interannual scale are still in debate. Here, we analyzed the time-series of FLUXCOM GPP (1980–2013), sun-induced fluorescence (SIF; 2001–2013) and site-level GPP measurements in three tropical evergreen forests regions (i.e., Amazon, Africa, and Southeast Asia). We decomposed the annual accumulated GPP into the basic and recurrent GPP, which represent the accumulated minimum and seasonal vegetation productivity, respectively. Then we quantified the proportion of each component and estimated the contribution to the IAV of GPP. We find that the basic GPP overwhelmed the recurrent GPP with the averaging ratio of 4.2:1 across the global tropical regions, and dominated the IAV of annual total GPP in 83.7% of the tropical evergreen forest areas. The high contribution of the basic GPP resulted from the great sensitivity of GPP_{min} to rainfall changes among years. The decomposition of the basic and recurrent GPP sheds new light on the understanding of tropical GPP variability in responding to climate change at seasonal and annual scale. Our study highlights the critical role of the GPP_{min} in shaping temporal dynamics of the annual GPP in tropical forests and emphasizes the importance of managing tropical forest of the shifting periods between wet-dry seasons in global tropical regions.

1. Introduction

Tropical forest, as one of the largest terrestrial biomes, contributes one-third of the total carbon uptake of the terrestrial biosphere (Beer et al., 2010), which offset 24% ~ 45% of the human carbon emissions during the past decades (Quéré et al., 2018). The year-to-year variations of carbon uptake by tropical forests substantially affect the global atmospheric CO_2 growth rate (Bacastow, 1976; Keeling & Revelle, 1985; Rayner and Law, 1999; Ahlström et al., 2015), the inter-annual variability (IAV) of the global carbon sink (Ahlström et al., 2015), and the sustainability of the global carbon boundaries (Stephens et al., 2007; Green et al., 2017). Thus, understanding the roles of external climate forcings and internal vegetation processes in influencing the IAV of tropical vegetation productivity becomes increasingly important.

Many previous studies have shown that precipitation controls the photosynthetic activities of tropical vegetation (Murphy and Lugo, 1986; Wright and Van Schaik, 1994; Malhi.Y., 2012), suggesting the important role of wet-season length in regulating GPP variability. However, some satellite-based observations have detected a greening trend of dry-season vegetation in tropical forests (Saleska et al., 2003; Huete et al., 2006; Brando et al., 2010; Guan et al., 2015; Saleska et al., 2016). Recently, sunlight has been recognized as a key driver of the increased photosynthesis during the dry season in tropical forests (Myneni et al., 2007; Huete et al., 2006; Samanta et al., 2012). With the ongoing controversy on the roles of precipitation and solar radiation in controlling seasonal productivity in tropical evergreen forests (Baker, 2008; Kim et al., 2012; Restrepo-Coupe et al., 2013; Morton et al., 2014; Wu et al., 2016), eddy-covariance measurements and near-surface remote sensing observations have further revealed the regulation of leaf demography on the seasonal GPP variability in Amazon (Brando

---

* Corresponding author.
E-mail address: jyxia@des.ecnu.edu.cn (J. Xia).

https://doi.org/10.1016/j.gloplacha.2020.103343
Received 1 April 2020; Received in revised form 6 October 2020; Accepted 8 October 2020

et al., 2010; Wu et al., 2016). All these findings have together underscored the importance of climatic and biophysiological factors (Wu et al., 2017) in mediating the variations of vegetation productivity in the tropical evergreen forests. However, which key internal process can explain the variations of the GPP crossing seasonal to decadal scales on the global tropical forests is far from clear (Guan et al., 2015; Ahlstrom et al., 2017; Wu et al., 2017; Huang et al., 2018).

In temperate and boreal ecosystems, growing season length is one of effective variables to indicate the variations of annual GPP (Linderholm, 2006; Wu et al., 2012; Barichivich et al., 2013; Chai et al., 2017; Li et al., 2018). The idealized seasonal GPP time-series, as bell-shaped curves (Gu et al., 2009; Xia et al., 2015), make it possible to decompose the temporal variability of GPP into the carbon uptake period (CUP) and the maximum photosynthesis capacity (GPP_{max}, Xia et al., 2015; Zhou et al., 2016). However, for the tropical evergreen ecosystems, photosynthetic activity is incompletely limited even under the worst natural environments (Restrepo-Coupe et al., 2013; Bi et al., 2015; Lopes et al., 2016; Wu et al., 2016), marking with a period of low-production rather than dormancy (Fig. 1). As well, weak correlations between GPP_{max} and annual total GPP in tropical regions were revealed by a global gridded analysis (Huang et al., 2018). Thus, the previous decomposition of annual GPP into CUP and GPP_{max} is unreasonable and invalid in explaining the GPP IAV in tropical evergreen ecosystems. A novel insight integrating eco-physiological and environmental drivers, as well as bridging the understanding of GPP variability on sub-annual and interannual time-scale in tropical evergreen ecosystems is urgently needed.

On the annual scale, yearly vegetation production is represented mathematically by the integral between the seasonal GPP curve and zero (Jönsson and Eklundh, 2004; Xia et al., 2015). The seasonal vegetation recurrence take place from the minimum productivity (GPP_{min}) level (Fig. 1), which represents the productivity-level could be achieved during the year-round with the seasonal changed physiological and environmental factors (Körner and Basler, 2010; Körner, 2015). Unlike ecosystems with a dormancy period or non-growing season (e.g. temperate deciduous forests), GPP_{min} in tropical forests, usually varies above zero (Jönsson and Eklundh, 2004; Gu et al., 2009; Richardson et al., 2013), causing a daily repeated GPP component for year-round (grey part in Fig. 1 c and d) and distinguishing the higher photosynthesis part as vegetation recurrence (green part in Fig. 1 c and d). Thus, the annual accumulated GPP could be decomposed into two components: one is the accumulation of the GPP_{min} during the whole year (here after, basic GPP), the other is the integral between the daily GPP and the GPP_{min} level, representing the accumulated seasonal vegetation productivity (here after, recurrent GPP).

As ratios between the basic and recurrent GPP on some extent represent the photosynthetic seasonality (Jönsson and Eklundh, 2004; Cleland et al., 2007) and the physiological effect of the integrated environments on vegetation productivity (Huete et al., 2006; Körner and Basler, 2010; Körner, 2015; Goll et al., 2018). The new decomposition of annual GPP into the basic and recurrent GPP show high potential to link the understanding of seasonal GPP variations with the inter-annual GPP variability. While, to the best of our knowledge, no analysis has been done to explore the role of GPP_{min} and the associated basic/recurrent GPP in determining the vegetation seasonality and affecting ecosystem functions such as annual productivity across the tropical regions.

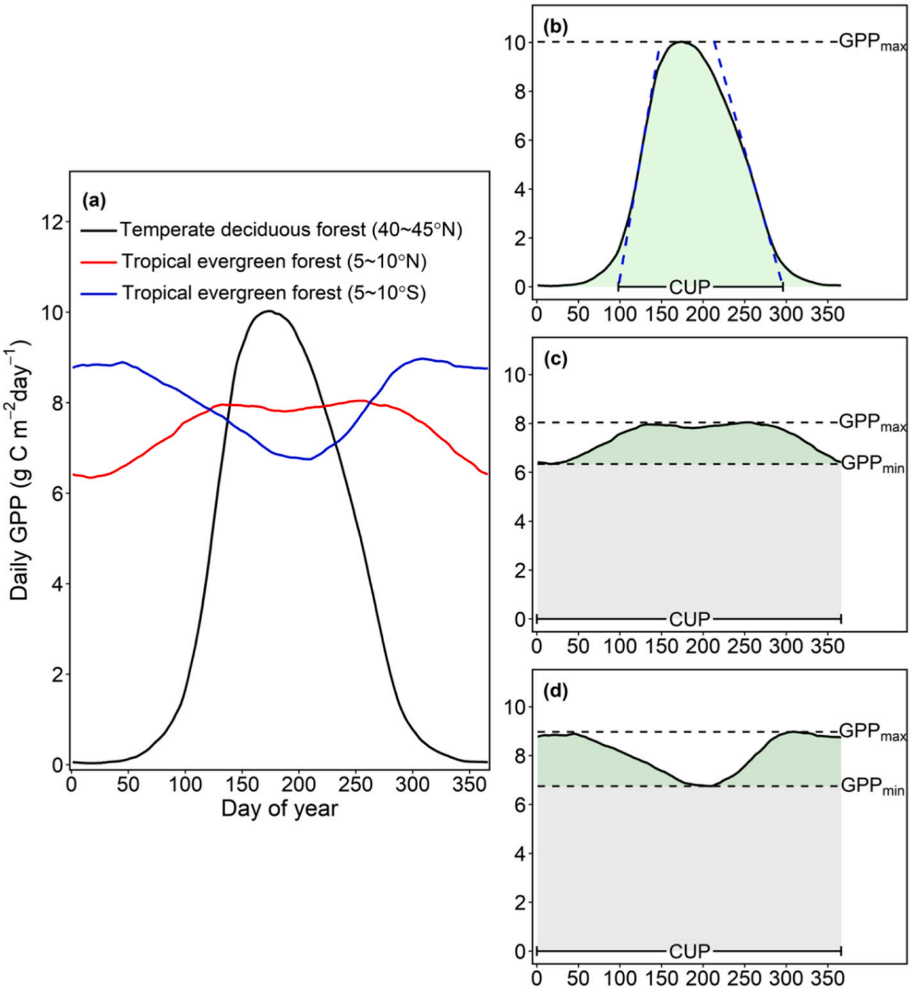

Fig. 1. Concept model. (a) Seasonal GPP curves for temporal deciduous forest (40– 45°N, black line), tropical evergreen forest in the northern hemisphere (5– 10°N, red line) and tropical evergreen forests in the southern hemisphere (5– 10°S, blue line). (b) Schematic for the joint control of CUP and GPP_{max} to annual GPP in temperate ecosystems. (c, d) Schematic for the decomposition of the annual GPP to the basic GPP and recurrent GPP for tropical evergreen forests in northern and southern hemispheres. For panels (b ~ d), the light green parts represent the recurrent GPP and the grey part show the basic GPP. (For interpretation of the references to colour in this figure legend, the reader is referred to the web version of this article.)

Here, mainly based on a 34-year-length (1980–2013) global GPP database (FLUXCOM), which merges tower measured eddy-covariance and satellite observations by three machine learning algorithms, we study the role of the basic GPP and recurrent GPP in regulating the GPP IAV in tropical forests. A continued sun-induced fluorescence (SIF) product from Orbiting Carbon Observatory-2 (OCO-2) and in-situ GPP based on partitioning of net ecosystems exchange (NEE) measurements from three eddy-flux towers in tropical forests were associated analyzed in this study. We aim to evaluate (1) proportions of the basic GPP and recurrent GPP separately; (2) contributions of the two components to the IAV in GPP; (3) how the climatic drivers regulate the GPP IAV by the changes of basic and recurrent GPP in tropic forests.

2. Materials and methods

2.1. Datasets

2.1.1. FLUXCOM GPP

FLUXCOM GPP is a model trained global GPP product which is upscaled from FLUXNET-based in situ eddy-covariance data from 224 flux towers (Valentini et al., 2014; Tramontana et al., 2016). First, the filtered and gap-filled daily NEE measurements were used to derive GPP through partitioning methods of Reichstein et al. (2005) and Lasslop et al. (2010). Then, these two sets of site-level GPP were independently used to train three machine learning models: Artificial Neural Networks (ANNs), Random Forest (RF), Model Trees Ensemble (MTE). For each model, 11 exploratory variables (New et al., 2000; Jung & Zscheischler 2013; Tramontana et al., 2016) with 0.5° spatial resolution and daily time step were selected as the driver data to predict the global GPP from 1980 to 2013. Combining these three machine learning algorithms with two flux partitioning methods, ensemble six sets of GPP estimates were provided (Jung et al., 2017). To exclude the uncertainties and biases across predictor models and partitioning methods, we used the daily GPP by the mean of all FLUXCOM ensemble members in this study.

2.1.2. FLUXNET GPP

Three flux sites from the FLUXNET2015 Dataset were selected to be used in this study, with below criteria: (1) located at the studied area (18°S to 12°N); (2) the continued recorded length is five years or longer; (3) the IGBP plant function type for that site is evergreen forest (both evergreen broadleaf forest and the evergreen needle-leaf forests are included). These three sites are Guyaflux (GF-Guy), Santarem-Km83-Logged Forest (BR-Sa3) and Pasoh Forest Reserve (MY-PSO), detailed information about these sites could be found in Table S1. In this study, night-time partitioning (Reichstein et al., 2005) GPP with daily step were used. The original time-series were first smoothed by spline method, then used to derive the maximum productivity (GPP_{max}) and the minimum productivity (GPP_{min}) for each site-year.

2.1.3. SIF product

Remotely sensed SIF data is a promising new global proxy for evaluating the canopy photosynthetic activity (Maxwell and Johnson, 2000; Baker, 2008). The continuous all-sky SIF dataset is gap-filled through a neural network (NN) model with the input variables of SIF retrievals at 757 nm from the Orbiting Carbon Observatory-2 (OCO-2) and daily Nadir Bidirectional reflectance distribution Adjust Reflectance from MODIS (MCD43C4 V006). The trained NN was validated to a coefficient of determination (R^2) around 0.8 (Zhang et al., 2018) at the spatial-temporal resolution of 0.05-degree and 4-days. Comparisons with the reconstructed all-sky SIF from GOME-2 and the eddy covariance-based GPP also support the reliability of this dataset (Zhang et al., 2018). In this study, to match with the FLUXCOM GPP, the all-sky SIF dataset with a 0.5-degree spatial resolution from the year 2001 to 2013 was used. To get the maximum and minimum values of the yearly SIF timeseries, the original data with 4-days-step was resampled to daily step and smoothed by spline method. Similar with that of the FLUXCOM and FLUXNET GPP, the maximum SIF (SIF_{max}) and minimum SIF (SIF_{min}) used in following analysis were derived from the smoothed timeseries.

2.1.4. Climate data

The Multi-satellite Precipitation Analysis from Tropical Measuring Mission Version 7 (TRMM 3B43 v7) was used in the hydrometeorological analyses. TRMM 3B43 v7 is a monthly dataset with a spatial resolution of 0.25° × 0.25°. It was calibrated by multiple satellite sensor measurements and gauge analyzed data, where feasible (Huffman et al., 2007). To match the resolution of GPP dataset, this rainfall data was resampled to 0.5° × 0.5°.

The CRU TS4.00 temperature (Harris and Jones, 2017) and gridded radiation dataset from the Terrestrial Hydrology Research Group at Princeton University (Sheffield et al., 2006) are used in the paper to conduct the analyses of GPP response. Both datasets are collected with a spatial resolution of 0.5° × 0.5° at monthly steps.

2.1.5. Plant function type distinctions

Plant functional types were distinguished using the annual MODIS land cover product (Friedl et al., 2010). This product, Land Cover Type Yearly L3 Global 500 m SIN Grid, with a short name of MCD12Q1, combines five global land cover classification systems. For this study, the evergreen tropical forest ecosystems are as a combination of evergreen broadleaf forest (EBF) and evergreen needle-leaf forest (ENF) between 18°S to 12°N.

2.2. Concept model

2.2.1. Seasonal curves

The daily GPP used for plotting the seasonal curves are first aggregated from the means of all eligible grid cells then averaged across the ensemble years. For example, the daily GPP used in plotting the seasonal curve for the temporal deciduous forests are averaged from all the grid cells marked as the deciduous needle-leaf forest (DNF) and the deciduous broadleaf forest (DBF) between 40°N ~ 45°N from 1980 to 2013 on each day. The same method used on the seasonal curves for tropical evergreen forests on both hemispheres. Seasonal curves in Fig. 2 for each tropical region plotted at each day are first averaged from all the grid cells marked as ENF and EBF in that region, then show the means and standard derivations (SD) across 1980–2013.

2.2.2. Definition for the basic GPP and recurrent GPP

As shown by Fig. 1, the basic GPP (grey part in Fig. 1 c, d) is defined as the integrals between the GPP_{min} level and zero-level for the whole year:

$$basic\ GPP = \sum_{1}^{DOY_{max}} GPP_{min} \tag{1}$$

And the recurrent GPP (green part in Fig. 1 c, d) is defined as the integrals between the daily GPP (GPP_{daily}) and the GPP_{min} level over the whole year, which could be mathematically represented as:

$$recurrent\ GPP = \sum_{1}^{DOY_{max}} \left(GPP_{daily} - GPP_{min}\right) \tag{2}$$

The DOY_{max} is the maximum Julian date of the year, which means 365 for normal years and 366 for leap years.

The combination of the basic GPP and the recurrent GPP is the annual accumulated GPP, which could also be understood as the integral between the daily GPP and the zero level.

2.2.3. Determination of GPP_{max} and GPP_{min}

The smoothing-spline approach (Hutchinson et al., 1985; Musial et al., 2011) was used to filter the outliers and obtain the daily smoothed GPP/SIF time series. This approach is applicable to a wide range of datasets and has been used in processing time series of various geophysical time series, such as the fraction of absorbed photosynthetic active radiation (FAPAR, Forkel et al., 2015) and vegetation indexes

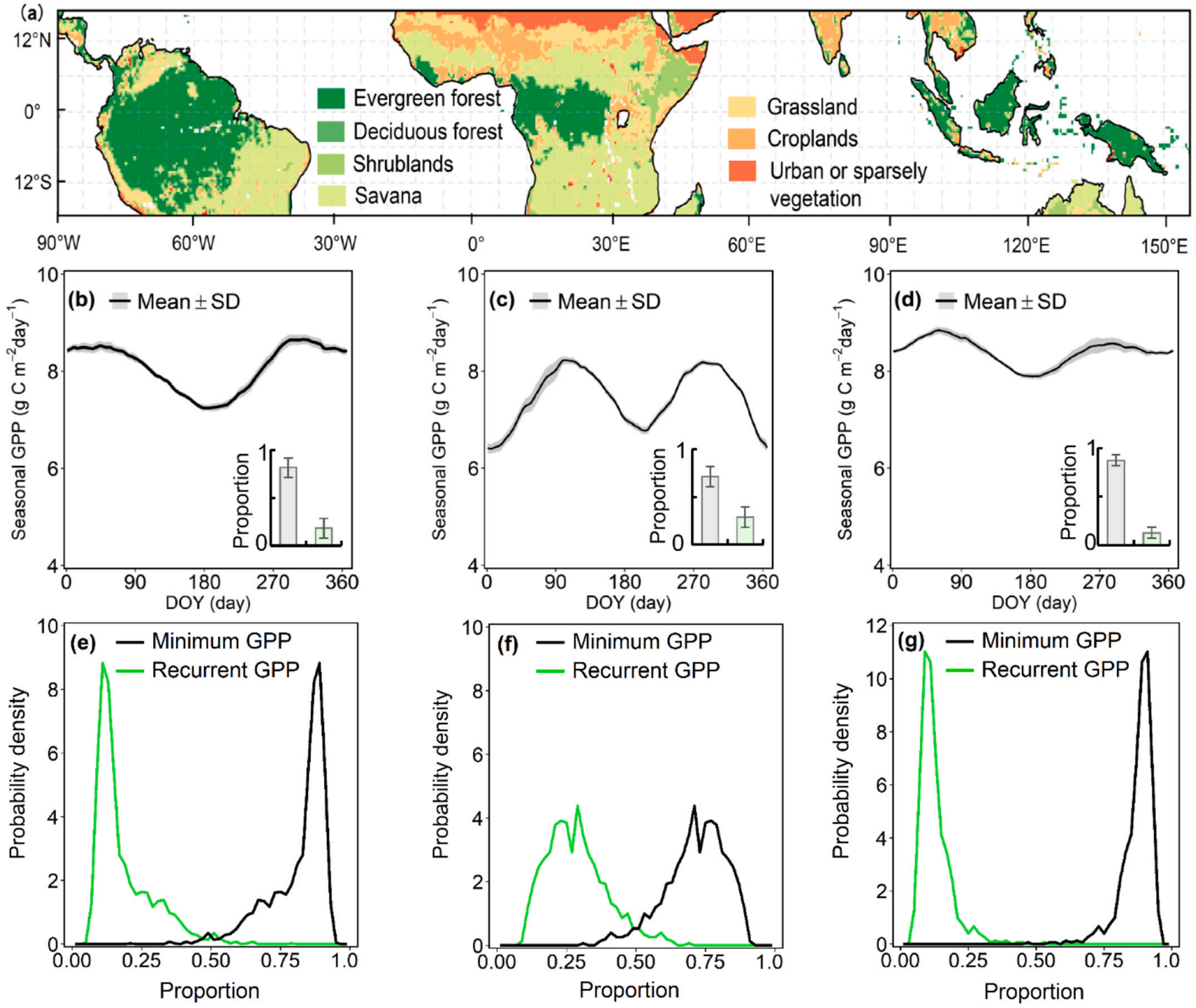

Fig. 2. Multi-year meaning proportions of the basic GPP and the recurrent GPP. (a) Plant function types in tropics. (b-d) Seasonal GPP curves of the evergreen forests in Amazon, Africa, and Southeast Asia. Blackline shows the multi-year average of each time-series, and shaded areas represent the stand deviation of daily GPP among these 34 years. The insert columns in each panel show the multi-year averaging fractions of the basic GPP (grey) and the recurrent GPP (light green) for each region. (e-c) The probability distribution functions (PDFs) of the proportions of the basic (black lines) and recurrent GPP (green lines) across all the grid-cells of evergreen forest in Amazon, Africa, and Southeast Asia. (For interpretation of the references to colour in this figure legend, the reader is referred to the web version of this article.)

(VIs, Keenan et al., 2014). The smoothed GPP time-series were latterly used to derive the GPP_{max}, GPP_{min} and to calculate the volume of the basic GPP and the recurrent GPP as the as Eq. (1) and (2) for each grid/site-year.

2.3. Analyses

2.3.1. Proportions of the basic and recurrent GPP

Proportions of the basic or recurrent GPP were first calculated on the grid-year scale as the ratio of the basic or recurrent GPP on the annual accumulated GPP. Then averages of the proportions from all grids during the study periods in that region were applied as the proportions of the basic/recurrent GPP of that region. Similar methods were used in the analysis for SIF. For the FLUXNET GPP, multi-year meaning proportions of the basic/recurrent GPP are the final proportions (in Table S1) for that site.

2.3.2. Contributions of the basic and recurrent GPP to GPP IAV

The approach of quantifying the relative contributions in Ahlström et al. (2015) was used here to scores the relative contributions of the basic and recurrent GPP to annual GPP IAV (Here after, *f* contribution):

$$f_i = \frac{\sum_t \frac{x_{it}|X_t|}{X_t}}{\sum_t \left|X_t\right|} \tag{3}$$

Where x_{it} is the anomalies (departure from a long-term trend) for component *i* at time *t* (in years), and X_t is the annual GPP anomalies, calculated as $X_t = \sum_i x_{it}$. With this method, the *f* contribution is the averaging relative anomalies of part *i* (x_{it}/X_t), weighted with the absolute annual GPP anomaly $|X_t|$.

To avoid the impact of biased volumes between the basic and recurrent GPP on the evaluation, the GPP time-series was first normalized by subtracting the climatic GPP_{min}, which is calculated as the minimum GPP_{min} during the standard climatological years (1981–2010). In this way, the standardized basic GPP (dark grey part in Fig. S1) is much less than the original basic GPP and the recurrent GPP. Then the *f* contributions were calculated for both basic and recurrent GPP on each grid cell. For each calculation, the higher and positive score is inferred to a larger contribution to the GPP IAV. Note that, for the evaluations on SIF and FLUXNET GPP, the standard climatological years being uncovered by the data duration. Therefore, the minimum SIF_{min}/GPP_{min} during the data duration was set as the climatic SIF_{min}/GPP_{min} and used to standardize the basic SIF/GPP.

2.3.3. Absolute variation and relative variation

The absolute variation was represented by the standard derivations (SD) and the relative variations are shown by the coefficient of variations (CV) here. The SD calculated as:

$$SD = \sqrt{\frac{1}{N}\sum_{1}^{N}(x-\mu)^2} \tag{4}$$

Meanwhile, the CV was defined as the ratio between SD and mean:

$$c_v = \frac{\sigma}{\mu} \tag{5}$$

2.3.4. Response of GPP to climatic factors

Slope of the temporal linear relationship between monthly GPP and monthly mean precipitation (radiation/temperature) is usually regarded as a proxy of the rainfall (radiation/temperature) sensitivity (Huxman et al., 2004; Hu et al., 2018). Here we used the downscaled scatter plot to show the response of the monthly GPP to climate gradients. Considering the lag-effect of climatic factors on vegetation, in these analyses, we first calculated the time lag for each variable on each grid cell following the method in Wu et al. (2015). Then the monthly rainfall (radiation/temperature) was calculated as averages of the rainfall (radiation/temperature) during the lag-effect month to the current month. For example, if the lag-time for the effect of rainfall on the GPP was 2 months, the monthly rainfall for that grid-cell used in the analysis would be the average value of the rainfall in that month, the last month and the last two months. Fig. S2 shows the lag-time.

3. Results

3.1. Proportions of the basic and recurrent GPP

The basic GPP overwhelmed the recurrent GPP in all the three regions, which was both detected by the FLUXCOM GPP and OCO-2 SIF (Figs. 2, 3 & S2). The basic GPP accounted for 82% of the total annual GPP in the Amazon, 71% in Africa and 87% in South East Asia. It was highly homogeneous in each region with the variations of 12.6% for the Amazon (across the total 2141 grids), 15.1% for Africa (across the total 753 grids) and 6.5% for South East Asia (across the totally 753 grids). Probability density functions showed that 90% quantiles for the proportion of the basic GPP concentrated around 79% ± 12%, 71% ± 14%, and 87% ± 6% separately for these three regions (Fig. 2). Greater proportions of the recurrent GPP than the basic GPP was found only in 1.6% of the studied grids in Amazon, 4.3% in Africa and 0.1% in South East Asia.

Similar results were shown by the SIF data, while the basic SIF overwhelming recurrent SIF is not as significant as that detected by the FLUXCOM GPP. Regionally averaged proportions for the basic SIF were separately detected as 76%, 56% and 74%, respectively being lower than the evaluations from FLUXCOM GPP, so as the 90% quantiles for the proportion of the basic SIF (Fig. S3). The higher proportions of the basic GPP could also be captured at the site-level. As shown by Table S1, the basic GPP in BR-Sa3 were detected as the highest proportions approximately 75%, 2.8 times of that for the recurrent GPP. Following with the sites GF-Guy and MY-PSO, the proportions of the basic GPP were found as 64% and 53.3%.

3.2. Contributions of the basic and recurrent GPP to GPP IAV

The contribution of basic GPP is higher than that of the recurrent GPP to the GPP IAV. At the regional scale, higher *f* contribution of basic GPP to the GPP IAV was found for all the three tropical regions (*f* contribution =1.51) and each individual region (1.46 for Amazon, 1.47 for Africa, 1.71 for Southeast Asia, Fig. 4). Higher contribution of basic GPP was found for 84.2% of all the studied grids (82.7% of the studied grids in Amazon, 83.4% in Africa and 89.2% in South East Asia, Fig. 4). On site-level, the basic GPP were detected as higher contributor than the recurrent GPP in all the three sites (Table S1). The site in Brazil show the highest contribution from recurrent GPP (0.22, Table S1).

The *f* contribution of basic SIF also shows significant advantages than that of the recurrent SIF in all three regions (Fig. 5b, S2). The *f* contributions of basic SIF center around 0.9 (the mode) across all the studied grids with a mean value of 1.23. The recurrent SIF negatively

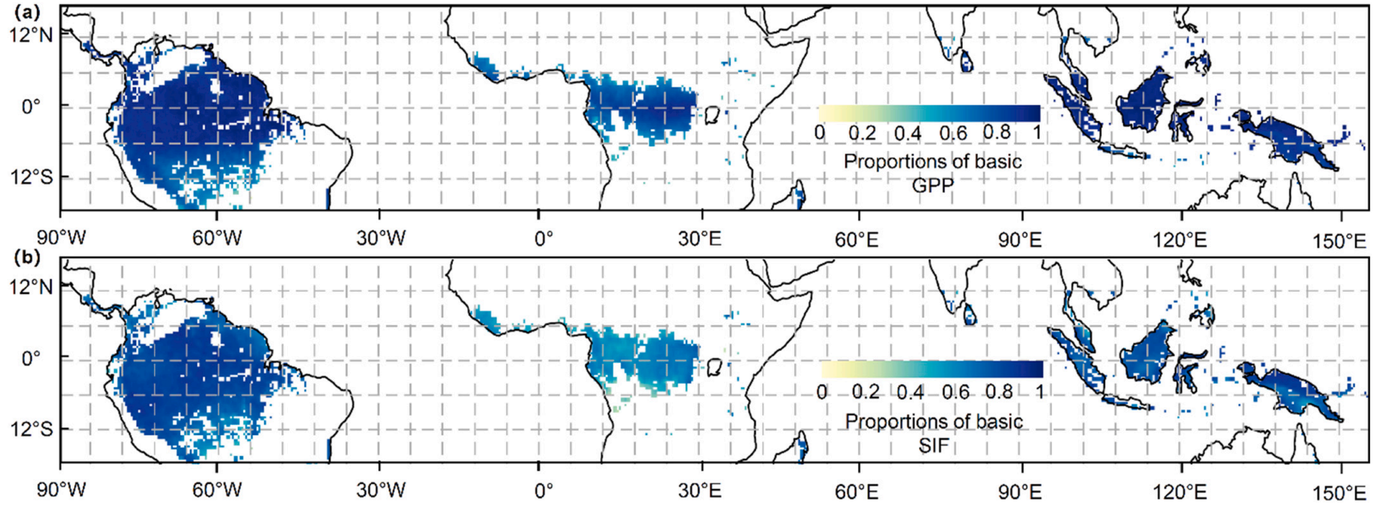

Fig. 3. Spatial pattern of the proportions for the basic GPP/SIF derived from the FLUXCOM GPP (a) and SIF (b).

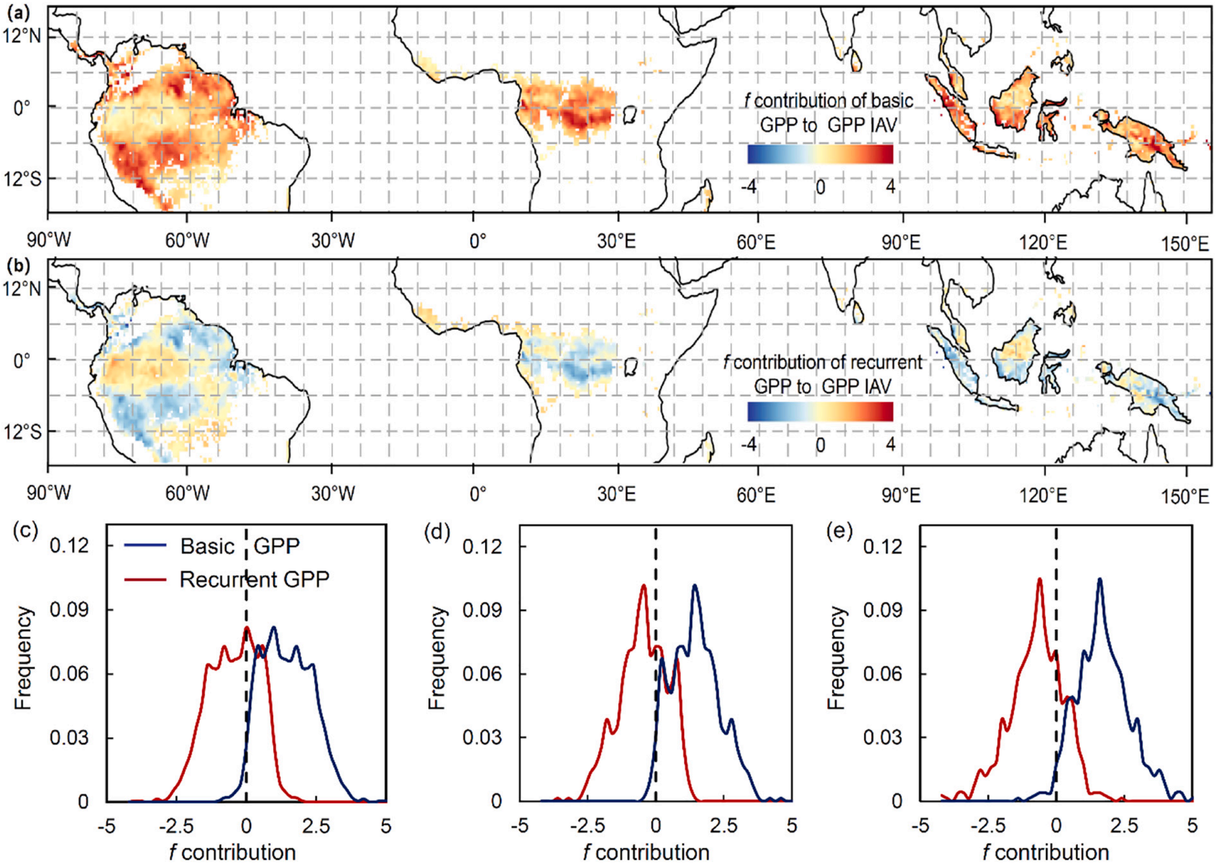

Fig. 4. Contributions of the basic GPP and recurrent GPP to GPP IAV. (a-b) Spatial maps for the contributions of the basic and recurrent GPP to GPP IAV. (c-d) The distribution frequency of the *f* contributions for each region.

contributed to the annual mean SIF IAV for 56.6% of the studied areas. The basic SIF controls the SIF IAV for 80.1% of the studied area in Amazon, 62.5% in Africa and 84.1% in Southeast Asia (77.3% of the whole studied areas, Fig. S4). Comparing with the results from GPP, the greatest discrepancies are shown in central Amazon (Fig. 4, S3), where the monthly mean precipitation is higher than 100 mm (Restrepo-Coupe et al., 2017). Considering the strong cloud activities in this area (Graham et al., 2003; Marthews et al., 2012; Zhu et al., 2018), the satellite derived SIF products are less recommended than the eddy-covariance upscaled GPP for the central Amazon.

3.3. Reasons for the dominance of basic GPP in GPP IAV

Considering the homogeneity of the mean annual temperature and solar radiation in the tropical zone (Restrepo-Coupe et al., 2013), we tested the rainfall impact on the magnitude and the variations of the basic and recurrent GPP spatially. The aggregated proportions and *f* contributions of these two components with rainfall gradients (Fig. 5) showed that the proportions for basic GPP increased with the higher mean annual precipitation (MAP) gradients both for GPP and SIF. Meanwhile, the widespread higher contribution of basic GPP to recurrent GPP is more obvious when it is aggregated by the precipitation bins (Fig. 5b, d). While no trends for the *f* contributions of basic GPP to GPP IAV were detected with the precipitation gradients. Negative contribution from recurrent component was found in areas with higher MAP, which show a MAP threshold of approximately 1500 mm yr^{-1} for GPP (Fig. 5b) and a MAP threshold of around 2000 mm yr^{-1} for SIF (Fig. 5d).

The yearly basic GPP is determined by the GPP$_{\text{min}}$ but the recurrent GPP is jointly determined by the daily GPP and the GPP$_{\text{min}}$, the increasing proportion of basic GPP with the MAP suggested asymmetric changing rates of the maximum daily production (represented by GPP$_{\text{max}}$ here) than the GPP$_{\text{min}}$ to the precipitation. As shown by Fig. 6, higher increments of the GPP$_{\text{min}}$ (SIF$_{\text{min}}$) than the GPP$_{\text{max}}$ (SIF$_{\text{max}}$) with the spatial precipitation gradients were found (Fig. 7a, c). Adopting this concept from space to time, higher SD and CV for GPP$_{\text{min}}$ (SIF$_{\text{min}}$) were generally revealed (Fig. S5, S6). As well, the variations of GPP$_{\text{min}}$ (SIF$_{\text{min}}$) were detected commonly lower than that of the GPP$_{\text{max}}$ (SIF$_{\text{max}}$) for all the MAP gradients (Fig. 6b, d), which caused the changes of the recurrent GPP (SIF) be opposite with that of the annual GPP and negatively contributed to the GPP (SIF) IAV in large areas.

The distinguishes between variations of the GPP$_{\text{max}}$ (SIF$_{\text{max}}$) and GPP$_{\text{min}}$ (SIF$_{\text{min}}$) could not be explained by the annual precipitation gradients (Fig. 6b, d; Fig. S7, S8). To check whether the precipitation in sub-annual level impact on the variations of GPP$_{\text{max}}$ (SIF$_{\text{max}}$) and GPP$_{\text{min}}$ (SIF$_{\text{min}}$), we further examined the response of GPP (SIF) to changes in environmental factors on the monthly scale. The downscaled scatter plot from all the month-girds (Fig. 7) illustrated the gradually declined response ratio of the monthly GPP (SIF) to the monthly precipitation. Consistent patterns for the response ratio of GPP$_{\text{min}}$ (SIF$_{\text{min}}$) to monthly precipitation were illustrated. Neutral response of GPP (SIF), GPP$_{\text{max}}$ (SIF$_{\text{max}}$) and GPP$_{\text{min}}$ (SIF$_{\text{min}}$) to monthly temperature was detected (Fig. S9). The changes of monthly GPP (SIF) and GPP$_{\text{min}}$ (SIF$_{\text{min}}$) increased gently at first but decreased sharply later with the increasing radiation (Fig. S9). The contrary response patterns of monthly GPP to radiation and precipitation changes were associated with the opposite seasonal patterns of the rainfall and radiation (Fig. S10).

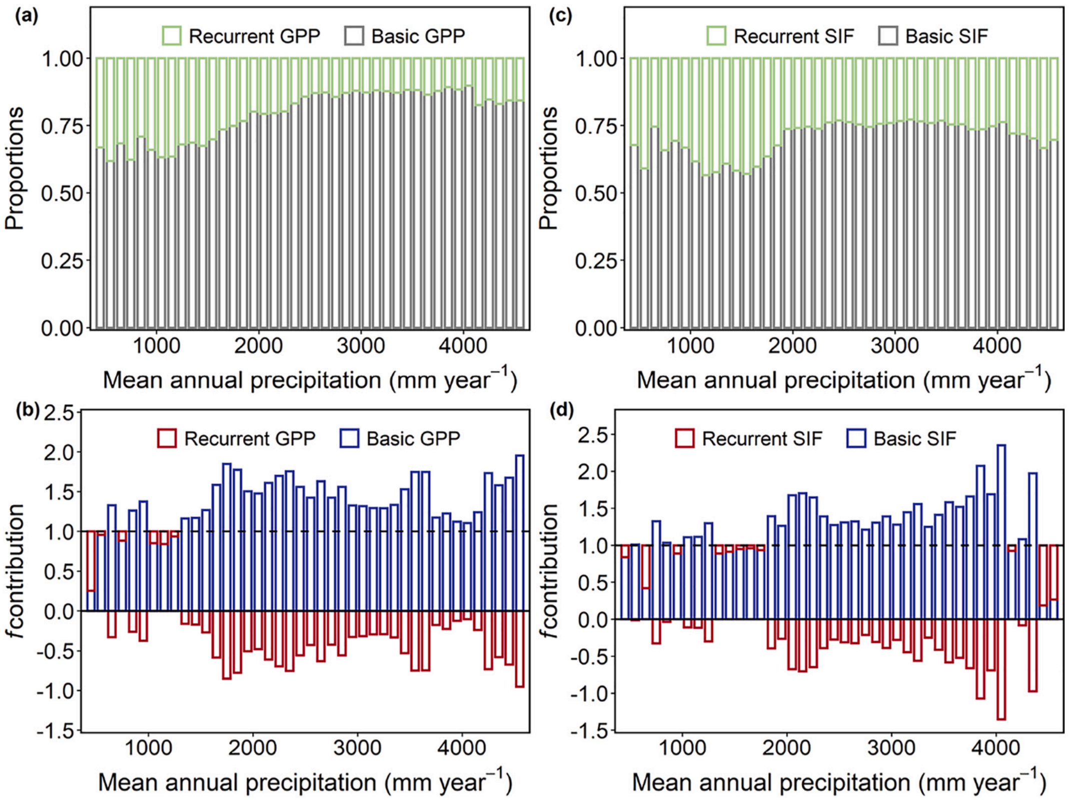

Fig. 5. Changes in the proportions (a, c) and contributions (b, d) of basic and the recurrent GPP (SIF) with MAP gradients. The upper panels show the proportions for the basic (grey columns) and the recurrent GPP/SIF (green columns) across all the studied grid-cells (a for FLUXCOM GPP; c for the SIF). The lower panels show the contributions of the basic (blue columns) and the recurrent GPP/SIF (red columns) across all the studied grid-cells (b for the FLUXCOM GPP; d for the SIF). Each column bin represents the annual rainfall of 100 mm year^{-1} here. (For interpretation of the references to colour in this figure legend, the reader is referred to the web version of this article.)

4. Discussion

4.1. *The conceptual model of decomposing GPP into basic and recurrent GPP*

Time-integrated areas of vegetation indexes (e.g., NDVI and EVI) have been used in previous studies (Rasmussen, 1992; Yang et al., 1998; Shi et al., 2017; Jin and Wang, 2016; Lai et al., 2018) to represent the yearly accumulated GPP. However, these applications are mostly employed in ecosystems with a distinct dormant season (Shi et al., 2017; Jin and Wang, 2016), in which all the photosynthetic product are totally recurrent. This implies severe an underestimated role of basic GPP in regulating the annual accumulated GPP, increasing the difficulties in capturing the seasonality of tropical evergreen vegetations (Xu et al., 2015; Restrepo-Coupe et al., 2017; Tian et al., 2018). The approach first puts the basic GPP in the front and reveals the large volumes and high variations of the basic GPP. It provides a new insight to research on the seasonal oscillations and the associated interannual variability of vegetation growth/productivity in tropical evergreen ecosystems.

One of the most disadvantages of this conceptual model is that biased weights are given to GPP_{max} and GPP_{min} in evaluating the contributions of the basic and recurrent GPP to GPP IAV. However, higher variations of GPP_{min} are the main causes of the higher variations of the basic GPP, because the absolute variations of GPP_{min} are much higher than those of GPP_{max} (Fig. S5). Differences between the relative variations of GPP_{min} and GPP_{max} are more obvious (Fig. S6), especially for the results aggregated by MAP bins (Fig. 6, S7).

4.2. *Dominant role of GPP_{min} in controlling the GPP IAV*

This study revealed that the GPP IAV in tropical evergreen forest is dominantly controlled by the basic GPP and the associated highly varied GPP_{min}. This result is inconsistent with some recent findings in extratropical ecosystems that the peak growth of vegetation contributes prominently both of the trends and IAV of the CO_2 uptake (Reichstein et al., 2014; Zhou et al., 2016; Zscheischler et al., 2016; Fu et al., 2017; Gonsamo et al., 2018). While, the tight relations for annual GPP and GPP_{min} other than that of the GPP_{max} in tropical evergreen ecosystems (Fig. S11) are definitely revealed.

Discrepancy between the variations of GPP_{min} and GPP_{max} is one-side caused by the non-uniform sensitivity of GPP_{min} and GPP_{max} to climatic factors (i.e., precipitation and solar radiations; Fig. 7, S8). In the other side, the high variations of precipitation during the low-GPP period also explain parts of the reasons (Fig. S12). As the variability of ecosystem productivity representing the inversed stability to disturbances (Tilman et al., 2006; Huang and Xia, 2019), the high variability of GPP_{min} and the high sensitivity of GPP_{min} to precipitation suggesting high risks of the status shift (Hu et al., 2018) when meet with intense or time-lasting drought events. Previous studies suggested to focus on the changing of dry season length (Fu et al., 2013; Guan et al., 2018; Sena et al., 2018) and the frequency of drought events during dry-seasons (Koren et al., 2018) to improve the sustainability and stabilities of the tropical ecosystems. However, the connecting period between wet and dry seasons, during which the GPP_{min} shows (Huete et al., 2006; Bi et al., 2015; Wu et al., 2016), are suggested more valuable to be focused by this study.

The low-varied GPP_{max} (Fig. 7) is hard to be attributed to the saturated photosynthesis capacity but to the limitation of the integrated environments for the tropical evergreen forests. Because the GPP_{max} in

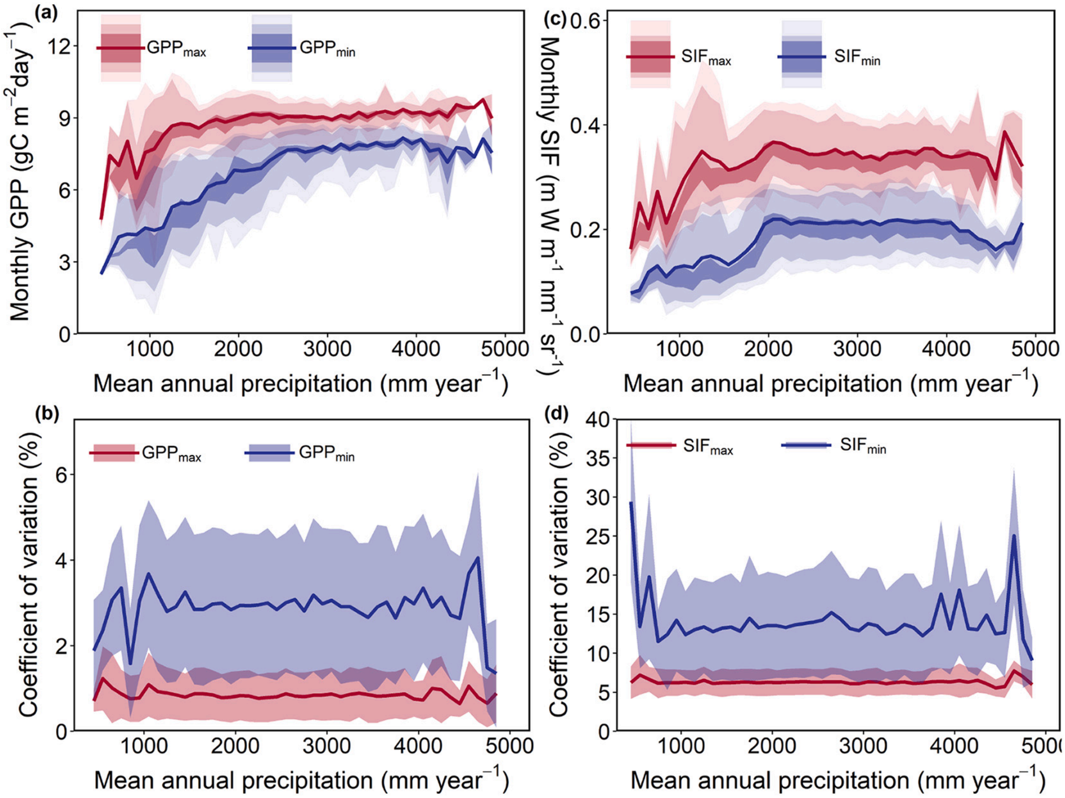

Fig. 6. Changes of the GPP_{max}/SIF_{max} and GPP_{min}/SIF_{min} with the MAP gradients. (a, c) Changes of the GPP_{max}/SIF_{max} (red) and GPP_{min}/SIF_{min} (blue) with the MAP gradients (a). The solid lines represent the mean values for each bin and shaded areas from light to dark separately show the percentage of 5% ~ 95%, 10% ~ 90% and 25% ~ 75% in each bin. (b, d) Relations between CV of the GPP_{max}/SIF_{max} (red) and GPP_{min}/SIF_{min} (blue) with the MAP gradients. CV is calculated as the variations of the GPP variables among 1980–2013 and of SIF variables among 2001–2013. The solid lines represent the mean values for each bin and shaded areas show the one SD variation for each bin. The width for all MAP bins here is 100 mm year^{-1}. (For interpretation of the references to colour in this figure legend, the reader is referred to the web version of this article.)

tropical forests is even lower than that of the temporal forests, which has been detected by other GPP products (e.g. VPM GPP, Zhang et al., 2018) and some in-situ measurements (Hirata et al., 2008). Desynchrony between peak radiation and water supply along with the deficit of nutrient supply (Corlett, 2016; Fleischer et al., 2019; Du et al., 2020) could limit further enhancement of the peak photosynthesis. Nutrient supplies from fertilization and nitrogen deposition enhanced the peak photosynthesis (Gray et al., 2014; Guanter et al., 2014; Huang et al., 2018) in the tropical human-managed ecosystems also providing the evidence for this (Sacks et al., 2009; Zeng et al., 2014; Zhang et al., 2015).

4.3. *The limitations and implications*

The analyses are mainly based on a machine learning translated gridded GPP dataset and associated by a satellite derived SIF product. Although machine-learning trained flux estimates give high reliability to the FLUXCOM products (Jung et al., 2017; Zhang et al., 2018), spatial noises of the GPP dataset are still high due to the strong heterogenization in tropical areas (Zhang et al., 2018; Stocker et al., 2019). Lacking available long-term in-situ measurements in Africa and South East Asia (Jung et al., 2017) and the irremovable cloudiness effect (Marthews et al., 2012) over the tropics add uncertainties on the accuracies of these datasets in tropics, as well as on findings in our study. Thus, more fundamental and long-term monitoring on ecological process are called for being established in Africa and South East Asia like that in Amazon forests (Wu et al., 2016).

A significant number of studies have illustrated the water and radiation co-limitation on vegetation growth in tropical forests (Malhi.Y., 2012; Saleska et al., 2016). Our findings, especially the asymmetric climatic responses between GPP_{max} and GPP_{min} at low MAP areas (Fig. 6), suggest the co-regulation of water and radiation on seasonal low-GPP (Fig. 7, S9). However, most state-of-the-art terrestrial biosphere models poorly represent the light regulations (e.g., light-harvesting adaptations and light driven leaf demography) on GPP (Malhado et al., 2009; Wu et al., 2016; Restrepo-Coupe et al., 2017). Such a limitation can cause mismatched seasonal cycles of GPP between the model outputs and observations at both site (Restrepo-Coupe et al., 2017) and regional levels (Fig. S13). To reliably predict the ecosystem response to future climate change, it is necessary to include the nonlinear eco-physiological effect of asynchronized climatic changes (i.e., temperature, precipitation and radiation).

Our study pays attention solely to the tropical evergreen forests, and the conceptual model of decomposing GPP into basic GPP and recurrent GPP is novel. In non-tropical regions, it has been widely reported that GPP_{max} jointly with CUP determines the annual GPP (Xia et al., 2015; Zhou et al., 2016; Fu et al., 2017). The revealed dominance of GPP_{min} for tropical GPP IAV poses a new question that how the dominant variable of GPP IAV shift from GPP_{max} to GPP_{min} globally with the decreasing latitudes or the reductive seasonality.

In summary, this study demonstrated a novel method to visualize the recurrence of vegetation productivity and explain the GPP IAV in tropical evergreen ecosystems. Through decomposing the GPP into the basic and recurrent components, we revealed the great contributions of GPP_{min} to both of the IAV of GPP in the global tropical evergreen forests. The asymmetric responses of GPP_{min} and GPP_{max} to precipitation are the main causes for the low variations in recurrent GPP and its contribution to the IAV of GPP. The highly varied GPP_{min} suggests a promising signal for monitoring and diagnosing the temporal dynamics of annual

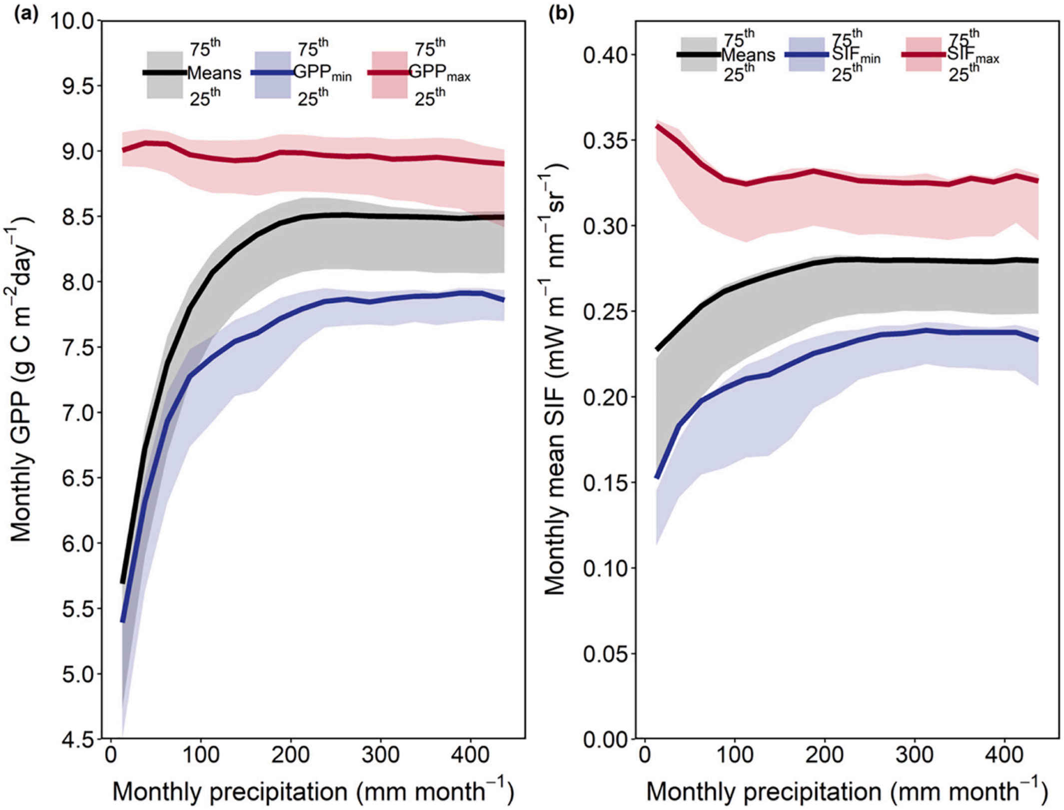

Fig. 7. Relationship between GPP (a)/SIF (b) and precipitation at the sub-annual scale. Changes in monthly GPP/SIF (black), GPP_{max}/SIF_{max} (red) and GPP_{min}/SIF_{min} (blue) along with monthly precipitation gradients (25 mm month^{-1} steps) for 1989–2013 (and 2001–2003 for SIF) across all the studied grids. Bold lines represent the mean values for the variables on each precipitation bin, and shade boundaries from top to bottom represent the third quartile and first quartile values of each variable on each precipitation bin. (For interpretation of the references to colour in this figure legend, the reader is referred to the web version of this article.)

productivity in tropical evergreen ecosystems.

Data availability

All data used for this study are publicly available online. The FLUXCOM GPP provided by Max Planck Institute for Biogeochemistry could be download from https://www.bgc-jena.mpg.de/geodb/projects/Home.php. Site-measured flux GPP is available from https://fluxnet.fluxdata.org/. The continuous gridded SIF data with a 0.5-degree spatial resolution could be obtained from https://figshare.com/articles/CSIF/6387494. The TRMM could get access from the NASA website ftp://disc2.nascom.nasa.gov/ftp/data/s4pa/TRMM_L3/TRMM_3B43. The original MODIS landcover data (MCD12Q1) are accessible from https://modis.gsfc.nasa.gov/data/dataprod/mod12.php. The model outputs of CMIP6 are obtained from https://esgf-node.llnl.gov/search/cmip6/.

Declaration of Competing Interest

None.

Acknowledgments

This work was financially supported by the National Key Research and Development Project (2017YFA0604600) National Natural Science Foundation of China (31722009, 31800400). This work was also financially supported by the China Scholarship Council (CSC) for Ph.D. students (201806140152). The authors acknowledge Dr. Wenxin Zhang & Dr. Torbern Tagesson for their constructive discussions and comments on the early version. We acknowledge FLUXNET, Max Planck Institute for Biogeochemistry and NASA for their work on the open datasets.

Appendix A. Supplementary data

Supplementary data to this article can be found online at https://doi.org/10.1016/j.gloplacha.2020.103343.

References

Ahlström, A., Raupach, M.R., Schurgers, G., Smith, B., Arneth, A., Jung, M., Kato, E., 2015. The dominant role of semi-arid ecosystems in the trend and variability of the land CO_2 sink. Science 348, 895–899.

Ahlstrom, A., Canadell, J., Schurgers, G., Orcid, I., Wu, M., Berry, JA, Jackson, R.B., 2017. Hydrologic resilience and Amazon productivity. Nature communication 8, 387.

Bacastow, R.B., 1976. Modulation of atmospheric carbon dioxide by the Southern Oscillation. Nature 261, 116–118.

Baker, N.R., 2008. Chlorophyll fluorescence: a probe of photosynthesis in vivo. Ann. Rev. Plant Biol. 59, 89–113.

Barichivich, J., Briffa, K.R., Myneni, R.B., Osborn, T.J., Melvin, T.M., Ciais, P., Tucker, C., 2013. Large-scale variations in the vegetation growing season and annual cycle of atmospheric CO_2 at high northern latitudes from 1950 to 2011. Global change biology 19, 3167–3183.

Beer, C., Reichstein, M., Tomelleri, E., Ciais, P., Jung, M., Carvalhais, N., Bondeau, A., 2010. Terrestrial gross carbon dioxide uptake: global distribution and covariation with climate. Science 329, 834–838.

Bi, J., Knyazikhin, Y., Choi, S., Park, T., Barichivich, J., Ciais, P., Huete, A., 2015. Sunlight mediated seasonality in canopy structure and photosynthetic activity of Amazonian rainforests. Environmental Research Letters 10, 064014.

Brando, P., Goetz, S.J., Baccini, A., Nepstad, D.C., Beck, P.S., Christman, M.C., 2010. Seasonal and interannual variability of climate and vegetation indices across the Amazon. Proc. Natl. Acad. Sci. USA 107, 14685–14690.

Chai, X., Shi, P., Zong, N., He, Y., Zhang, X., Xu, M., Zhang, J., 2017. A growing season climatic index to simulate gross primary productivity and carbon budget in a Tibetan alpine meadow. Ecol. Indic. 81, 285–294.

Cleland, E.E., Chuine, I., Menzel, A., Mooney, H.A., Schwartz, M.D., 2007. Shifting plant phenology in response to global change. Trends Ecol. Evol. 22, 357–365.

Corlett, R.T., 2016. Tropical forest ecosystem ecology: water, energy, carbon, and nutrients. Trop. Forest. Handbook 491–501.

Du, E., Terrer, C., Pellegrini, A.F., Ahlström, A., van Lissa, C.J., Zhao, X., Jackson, R.B., 2020. Global patterns of terrestrial nitrogen and phosphorus limitation. Nature Geoscience 13, 221–226.

Fleischer, K., Rammig, A., De Kauwe, M.G., Walker, A.P., Domingues, T.F., Fuchslueger, L., Haverd, V., 2019. Amazon forest response to CO_2 fertilization dependent on plant phosphorus acquisition. Nature Geoscience 12, 736–741.

Forkel, M., Migliavacca, M., Thonicke, K., Reichstein, M., Schaphoff, S., Weber, U., Carvalhais, N., 2015. Codominant water control on global interannual variability and trends in land surface phenology and greenness. Glob. Chang. Biol. 21, 3414–3435.

Friedl, M.A., Sulla-Menashe, D., Tan, B., Schneider, A., Ramankutty, N., Sibley, A., Huang, X., 2010. MODIS Collection 5 global land cover: Algorithm refinements and characterization of new datasets. Remote Sens. Environ. 1141, 68–182.

Fu, Z., Dong, J., Zhou, Y., Stoy, P.C., Niu, S., 2017. Long term trend and interannual variability of land carbon uptake—the attribution and processes. Environ. Res. Lett. 12, 014018.

Fu, R., Yin, L., Li, W., Arias, P.A., Dickinson, R.E., Huang, L., Myneni, R.B., 2013. Increased dry-season length over southern Amazonia in recent decades and its implication for future climate projection. Proc. Natl. Acad. Sci. 110, 18110–18115.

Goll, D.S., Joetzjer, E., Huang, M., Ciais, P., 2018. Low Phosphorus Availability Decreases Susceptibility of Tropical primary Productivity to Droughts. Geophys. Res. Lett. 45, 8231–8240.

Gonsamo, A., Chen, J.M., Ooi, Y.W., 2018. Peak season plant activity shift towards spring is reflected by increasing carbon uptake by extratropical ecosystems. Glob. Chang. Biol. 24, 2117–2128.

Graham, E.A., Mulkey, S.S., Kitajima, K., Phillips, N.G., Wright, S.J., 2003. Cloud cover limits net CO_2 uptake and growth of a rainforest tree during tropical rainy seasons. Proc. Natl. Acad. Sci. USA 100, 572–576.

Gray, J.M., Frolking, S., Kort, E.A., Ray, D.K., Kucharik, C.J., Ramankutty, N., Friedl, M. A., 2014. Direct human influence on atmospheric CO_2 seasonality from increased cropland productivity. Nature 515, 398–401.

Green, J.K., Konings, A.G., Alemohammad, S.H., Berry, J., Entekhabi, D., Kolassa, J., Gentine, P., 2017. Regionally strong feedbacks between the atmosphere and terrestrial biosphere. Nature Geoscience 10, 410.

Gu, L, Post, W.M., Baldocchi, D.D., Black, T.A., Suyker, A.E., Verma, S.B., Wofsy, S.C., 2009. Characterizing the seasonal dynamics of plant community photosynthesis across a range of vegetation types.Phenology of Ecosystem Processes. Springer, pp. 35–58.

Guan, K., Pan, M., Li, H., Wolf, A., Wu, J., Medvigy, D., Liang, M., 2015. Photosynthetic seasonality of global tropical forests constrained by hydroclimate. Nature. Geoscience 8, 284–289.

Guan, K., Good, S.P., Caylor, K.K., Medvigy, D., Pan, M., Wood, E.F., Xu, X., 2018. Simulated sensitivity of African terrestrial ecosystem photosynthesis to rainfall frequency, intensity, and rainy season length. Environmental Research Letters 13, 025013.

Guanter, L., Zhang, Y., Jung, M., Joiner, J., Voigt, M., Berry, J.A., Moran, M.S, 2014. Global and time-resolved monitoring of crop photosynthesis with chlorophyll fluorescence. Proc. Natl. Acad. Sci. USA 111, 1327–1333.

Harris, I.C., Jones, P.D., 2017. University of East Anglia Climatic Research Unit 2017CRUTS4.00: Climatic Research Unit (CRU) Time-Series (TS) Version 4.00 of High-Resolution Gridded Data of Month-by-Month Variation in Climate (Jan. 1901-Dec. 2015). Centre for Environmental Data Analysis, Chilton, Oxfordshire.

Hirata, R., Saigusa, N., Yamamoto, S., Ohtani, Y., Ide, R., Asanuma, J., Li, S.G., 2008. Spatial distribution of carbon balance in forest ecosystems across East Asia. Agricultural and Forest Meteorology 148, 761–775.

Hu, Z., Guo, Q., Li, S., Piao, S., Knapp, A.K., Ciais, P., Yu, G., 2018. Shifts in the dynamics of productivity signal ecosystem state transitions at the biome-scale. Ecology letters 21, 1457–1466.

Huang, K., Xia, J., 2019. High ecosystem stability of evergreen broadleaf forests under severe droughts. Glob. Chang. Biol. 25, 3494–3503.

Huang, K., Xia, J., Wang, Y., Ahlström, A., Chen, J., Cook, R.B., Yiq, L., 2018. Enhanced peak growth of global vegetation and its key mechanisms. Natl. Ecol. Evol. 2, 1897.

Huete, A.R., Didan, K., Shimabukuro, Y.E., Ratana, P., Saleska, S.R., Hutyra, L.R., Myneni, R., 2006. Amazon rainforests green-up with sunlight in dry season. Geophysical research letters 2006, 33.

Huffman, G.J., Bolvin, D.T., Nelkin, E.J., Wolff, D.B., Adler, R.F., Gu, G., Stocker, E.F., 2007. The TRMM multisatellite precipitation analysis (TMPA): quasi-global, multiyear, combined-sensor precipitation estimates at fine scales. Journal of Hydrometeorolgy 8, 38–55.

Huxman, T.E., Smith, M.D., Fay, P.A., Knapp, A.K., Shaw, M.R., Loik, M.E., Pockman, W. T., 2004. Convergence across biomes to a common rain-use efficiency. Nature 429, 651–654.

Jin, J., Wang, Q., 2016. Assessing ecological vulnerability in western China based on Time-Integrated NDVI data. J. Arid Land 8, 533–545.

Jönsson, P., Eklundh, L., 2004. TIMESAT—a program for analyzing time-series of satellite sensor data. Comput. Geosci. 30, 833–845.

Jung, M., Reichstein, M., Schwalm, C.R., Huntingford, C., Sitch, S., Ahlström, A., Arneth, A., Camps-Valls, G., Ciais, P., Friedlingstein, P., Gans, F., Ichii, K., Jain, A.K., Kato, E., Papale, D., Poulter, B., Raduly, B., Rödenbeck, C., Tramontana, G., Viovy, N., Wang, Y.-P., Weber, U., Zaehle, S., Zeng, N., 2017. Compensatory water effects link yearly global land CO_2 sink changes to temperature. Nature 541, 516–520.

Keeling, C.D., Revelle, R., 1985. Effects of El Nino/Southern Oscillation on the atmospheric content of carbon dioxide. Meteoritics 20, 437–450.

Keenan, T.F., Gray, J., Friedl, M.A., Toomey, M., Bohrer, G., Hollinger, D.Y., Yang, B., 2014. Net carbon uptake has increased through warming-induced changes in temperate forest phenology. Nature Climate Change 4, 598–604.

Kim, Y., Knox, Ryan G., Longo, Marcos, Medvigy, David, Hutyrak, Lucy R., Pyle, Elizabeth H., Wofsy, Steven C., Bras, Rafael, Moorcroft, Paul R., 2012. Seasonal carbon dynamics and water fluxes in an Amazon rainforest. Glob. Chang. Biol. 18, 1322–1334.

Koren, G., van Schaik, E., Araújo, A.C., Boersma, K.F., Gärtner, A., Killaars, L., Smith, N. E., 2018. Widespread reduction in sun-induced fluorescence from the Amazon during the 2015/2016 El Niño. Philos. Trans. Royal Society B 373, 20170408.

Körner, C., 2015. Paradigm shift in plant growth control. Curr. Opin. Plant Biol. 25, 107–114.

Körner, C., Basler, D., 2010. Phenology under global warming. Science 327, 1461–1466.

Lai, Y.R., Pringle, M.J., Kopittke, P.M., Menzies, N.W., Orton, T.G., Dang, Y.P., 2018. An empirical model for prediction of wheat yield, using time-integrated Landsat NDVI. Int. J. Appl. Earth Obs. Geoinf. 72, 99–108.

Lasslop, G., Reichstein, M., Papale, D., Richardson, A.D., Arneth, A., Barr, A., Stoy, P., Wohlfahrt, G., 2010. Separation of net ecosystem exchange into assimilation and respiration using a light response curve approach: critical issues and global evaluation. Glob. Chang. Biol. 16, 187–208.

Li, Z., Xia, J., Ahlström, A., Rinke, A., Koven, C., Hayes, D.J., Cheng, W., 2018. Non-uniform seasonal warming regulates vegetation greening and atmospheric CO_2 amplification over northern lands. Environmental Research Letters 13, 124008.

Linderholm, H.W., 2006. Growing season changes in the last century. Agric. For. Meteorol. 137, 1–14.

Lopes, A.P., Nelson, B.W., Wu, J., de Alencastro Graça, P.M. L., Tavares, J.V., Prohaska, N., Saleska, S.R., 2016. Leaf flush drives dry season green-up of the Central Amazon. Remote Sensing of Environment 182, 90–98.

Malhado, C.H.M., Carneiro, P.L.S., Affonso, P.R.A.M., Souza Jr., A.A.O., Sarmento, J.L.R., 2009. Growth curves in Dorper sheep crossed with the local Brazilian breeds, Morada Nova, Rabo Largo, and Santa Inês. Small Rumin. Res. 84, 16–21.

Malhi.Y., 2012. The productivity, metabolism and carbon cycle of tropical forest vegetation. J. Ecol. 100, 65–75.

Marthews, T.R., Malhi, Y., Iwata, H., 2012. Calculating downward longwave radiation under clear and cloudy conditions over a tropical lowland forest site: an evaluation of model schemes for hourly data. Theor. Appl. Climatol. 107, 461–477.

Maxwell, K., Johnson, G.N., 2000. Chlorophyll fluorescence—a practical guide. J. Exp. Bot. 51, 659–668.

Murphy, P.G., Lugo, A.E., 1986. Ecology of tropical dry forest. Annu. Rev. Ecol. Syst. 17, 67–88.

Myneni, R.B., Yang, W., Nemani, R.R., Huete, A.R., Dickinson, R.E., Knyazikhin, Y., Hashimoto, H., 2007. Large seasonal swings in leaf area of Amazon rainforests. Proc. Natl. Acad. Sci. USA 104, 4280–4823.

Morton, D.C, Nagol, J., Carabajal, C.C., Rosette, J., Palace, M., Cook, B.D., North, P.R., 2014. Amazon forests maintain consistent canopy structure and greenness during the dry season. Nature 506, 221.

New, M., Hulme, M., Jones, P., 2000. Representing twentieth-century space-time climate variability. Part II: Development of 1901-96 monthly grids of terrestrial surface climate. J. Clim. 13, 2217–2238.

Quéré, C., Andrew, R., Friedlingstein, P., Sitch, S., Hauck, J., Pongratz, J., Arneth, A., 2018. Global carbon budget 2018. Earth System Science Data 10, 2141–2194.

Rasmussen, M.S., 1992. Assessment of millet yields and production in northern Burkina Faso using integrated NDVI from the AVHRR. Int. J. Remote Sens. 13, 3431–3442.

Rayner, P.J., Law, R.M., 1999. The interannual variability of the global carbon cycle. Tellus B Chem. Phys. Meteorol. 51 (2), 210–212.

Reichstein, M., Falge, E., Baldocchi, D., Papale, D., Aubinet, M., Berbigier, P., Bernhofer, C., Buchmann, N., Gilmanov, T., Granier, A., 2005. On the separation of net ecosystem exchange into assimilation and ecosystem respiration: review and improved algorithm. Glob. Chang. Biol. 11, 1424–1439.

Reichstein, M., Bahn, M., Mahecha, M.D., Kattge, J., Baldocchi, D.D., 2014. Linking plant and ecosystem functional biogeography. Proc. Natl. Acad. Sci. USA 111, 13697–13702.

Restrepo-Coupe, N., da Rocha, H.R., Hutyra, L.R., da Araujo, A.C., Borma, L.S., Christoffersen, B., Fitzjarrald, D.R., 2013. What drives the seasonality of photosynthesis across the Amazon basin? A cross-site analysis of eddy flux tower measurements from the Brasil flux network. Agric. Forest Meteorol. 182, 128–144.

Restrepo-Coupe, N., Levine, N.M., Christoffersen, B.O., Albert, L.P., Wu, J., Costa, M.H., Malhi, Y.S., 2017. Do dynamic global vegetation models capture the seasonality of carbon fluxes in the Amazon basin? A data-model intercomparison. Global Change Biology 23, 191–208.

Richardson, A.D., Keenan, T.F., Migliavacca, M., Ryu, Y., Sonnentag, O., Toomey, M., 2013. Climate change, phenology, and phenological control of vegetation feedbacks to the climate system. Agric. Forest Meteorol. 169, 156–173.

Saleska, S.R, Miller, S.D, Matross, D.M, Goulden, M.L, Wofsy, S.C, de Rocha, H.R., Silva, H., 2003. Carbon in Amazon forests: unexpected seasonal fluxes and disturbance-induced losses. Science 302, 1554–1557.

Sacks, W.J., Cook, B.I., Buenning, N., Levis, S., Helkowski, J.H., 2009. Effects of global irrigation on the near-surface climate. Climate. Dynamics 33, 159–175.

Saleska, S.R., Wu, J., Guan, K., Araujo, A.C., Huete, A., Nobre, A.D., Restrepo-Coupe, N., 2016. Dry-season greening of Amazon forests. Nature 531, E4–E5.

Samanta, A., Knyazikhin, Y., Xu, L., Dickinson, R.E., Fu, R., Costa, M.H., Myneni, R.B., 2012. Seasonal changes in leaf area of Amazon forests from leaf flushing and abscission. J. Geophys. Res. 117 (G1).

Sena, E.T., Dias, M.S., Carvalho, L.M.V., Dias, P.S., 2018. Reduced wet-season length detected by satellite retrievals of cloudiness over Brazilian Amazonia: a new methodology. J. Clim. 31, 9941–9964.

Sheffield, J., Goteti, G., Wood, E.F., 2006. Development of a 50-year high-resolution global dataset of meteorological forcings for land surface modeling. J. Clim. 19, 3088–3111.

Shi, H., Li, L., Eamus, D., Huete, A., Cleverly, J., Tian, X., Rotenberg, E., 2017. Assessing the ability of MODIS EVI to estimate terrestrial ecosystem gross primary production of multiple land cover types. Ecological indicators 72, 153–164.

Stephens, B.B., Gurney, K.R., Tans, P.P., Sweeney, C., Peters, W., Bruhwiler, L., Aoki, S., 2007. Weak northern and strong tropical land carbon uptake from vertical profiles of atmospheric CO_2. Science 316, 1732–1735.

Stocker, B.D., Zscheischler, J., Keenan, T.F., Prentice, I.C., Seneviratne, S.I., Peñuelas, J., 2019. Drought impacts on terrestrial primary production underestimated by satellite monitoring. Nat. Geosci. 12, 264.

Tian, F., Wigneron, J.P., Ciais, P., Chave, J., Ogée, J., Penuelas, J., Mialon, A., 2018. Coupling of ecosystem-scale plant water storage and leaf phenology observed by satellite. Nat. Ecol. Evolut. 2, 1428–1435.

Tilman, D., Reich, P.B., Knops, J.M.H., 2006. Biodiversity and ecosystem stability in a decade-long grassland experiment. Nature 441, 629–632.

Tramontana, G., Jung, M., Schwalm, C.R., Ichii, K., Camps-Valls, G., Ráduly, B., Reichstein, M., Papale, D., 2016. Predicting carbon dioxide and energy fluxes across global FLUXNET sites with regression algorithms. Biogeosciences 13, 4291–4313.

Valentini, R., Arneth, A., Bombelli, A., Castaldi, S., Cazzolla Gatti, R., Chevallier, F., Henry, M., 2014. A full greenhouse gases budget of Africa: synthesis, uncertainties, and vulnerabilities. Biogeosciences 11, 381–407.

Wright, S.J., Van Schaik, C.P., 1994. Light and the phenology of tropical trees. Am. Nat. 143, 192–199.

Wu, C., Gonsamo, A., Chen, J.M., Kurz, W.A., Price, D.T., Lafleur, P.M., Verma, S.B., 2012. Interannual and spatial impacts of phenological transitions, growing season length, and spring and autumn temperatures on carbon sequestration: A North America flux data synthesis. Global and Planetary Change 92, 179–190.

Wu, D., Zhao, X., Liang, S., Zhou, T., Huang, K., Tang, B., Zhao, W., 2015. Time-lag effects of global vegetation responses to climate change. Glob. Chang. Biol. 21, 3520–3531.

Wu, J., Albert, L.P., Lopes, A.P., Restrepo-Coupe, N., Hayek, M., Wiedemann, K.T., Tavares, J.V., 2016. Leaf development and demography explain photosynthetic seasonality in Amazon evergreen forests. Science 351, 972–976.

Wu, J., Guan, K., Hayek, M., Restrepo-Coupe, N., Wiedemann, K.T., Xu, X., Wehr, R., Christoffersen, B.O., Miao, G., da Silva, R., de Araujo, A.C., Oliviera, R.C., Camargo, P.B., Monson, R.K., Huete, A.R., Saleska, S.R., 2017. Partitioning controls on Amazon forest photosynthesis between environmental and biotic factors at hourly to interannual timescales. Glob. Chang. Biol. 23, 1240–1257.

Xia, J., Niu, S., Ciais, P., Janssens, I.A., Chen, J., Ammann, C., Buchmann, N., 2015. Joint control of terrestrial gross primary productivity by plant phenology and physiology. Proc. Natl. Acad. Sci. 112, 2788–2793.

Xu, L., Saatchi, S.S., Yang, Y., Myneni, R.B., Frankenberg, C., Chowdhury, D., Bi, J., 2015. Satellite observation of tropical forest seasonality: spatial patterns of carbon exchange in Amazonia. Environ. Res. Lett. 10, 084005.

Yang, L., Wylie, B.K., Tieszen, L.L., Reed, B.C., 1998. An analysis of relationships among climate forcing and time-integrated NDVI of grasslands over the US northern and central Great Plains. Remote Sens. Environ. 65, 25–37.

Zeng, N., Zhao, F., Collatz, G.J., Kalnay, E., Salawitch, R.J., West, T.O., Guanter, L., 2014. Agricultural Green Revolution as a driver of increasing atmospheric CO_2 seasonal amplitude. Nature 515, 394–397.

Zhang, X., Davidson, E.A., Mauzerall, D.L., Searchinger, T.D., Dumas, P., Shen, Y., 2015. Managing nitrogen for sustainable development. Nature 528, 51–59.

Zhang, Y., Joiner, J., Alemohammad, S.H., Zhou, S., Gentine, P., 2018. A global spatially contiguous solar-induced fluorescence (CSIF) dataset using neural networks. Biogeosciences 15, 5779–5800.

Zhou, S., Zhang, Y., Caylor, K.K., Luo, Y., Xiao, X., Ciais, P., Wang, G., 2016. Explaining inter-annual variability of gross primary productivity from plant phenology and physiology. Agric. Forest Meteorol. 226, 246–256.

Zhu, J., Zhang, M., Zhang, Y., Zeng, X., Xiao, X., 2018. Response of tropical terrestrial gross primary production to the super El Niño event in 2015. J. Geophys. Res. 123, 3193–3203.

Zscheischler, J., Fatichi, S., Wolf, S., Blanken, P.D., Bohrer, G., Clark, K., Seneviratne, S. I., 2016. Short-term favorable weather conditions are an important control of interannual variability in carbon and water fluxes. J. Geophys. Res. 121, 2186–2198.